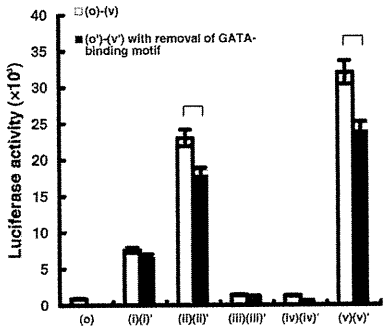

Figure 4. The GATA2-binding motif and retroviral promoter activity in luciferase assays. Relative luciferase activity is shown using vector constructs consisting of native or GATA2 motif defective flanking sequences. Individual assays were independently performed five times. The activity ratios (Firefly to Renilla luciferase) of **ii** and **v** were significantly higher than those of **ii**′ and **v**′, respectively (**ii** versus **ii**′, $^{*}P = 0.031$; **v** versus **v**′, $^{**}P = 0.028$). Measurements of luciferase activity were performed five times using individual vectors. Luciferase activity values were evaluated using the Student's *t*-test.

TATC-3′ was observed in integration site 1130 of the *Stat5a* sequence that was included in vectors i, ii, iii, iv, and v (Figure 2A). To evaluate the contribution of the motif to luciferase activity, assays were performed using five modified vectors (i′, ii′, iii′, iv′, and v′) from which the GATA2-binding motif in i, ii, iii, iv, and v, respectively, had been removed. The results revealed that luciferase activity was significantly higher when vectors ii and v were used relative to when vectors ii′ and v′, respectively, were used (Figure 4).

IP of Transcriptional Factor Binding to the Provirus-Stat5a Junction

We performed an IP assay using lymphoma clones and antibodies against proteins that have the potential to bind to LTR or the flanking sequences. The results revealed that Runx1 and integrase, GATA2 and integrase, GATA2 and p300, CREB-P1 and GATA2, and CREB-P1 and p300 form complexes (Figure 5A). Moreover, ChIP was performed using antibodies against Runx1, GATA2, and integrase. The precipitated DNA included *Emv11* 3′-LTR-*Stat5a* fusion genomic DNA in the Stat5a^{high} clones (Figure 5B). Moreover, reperformed IP of DNA fragments that were precipitated by an antibody against GATA2 or GATA1 was done using an antibody against Runx1 and p300. The results revealed that the *Emv11*-3′-LTR-*Stat5a* segment was coimmunoprecipitated with GATA2-Runx1

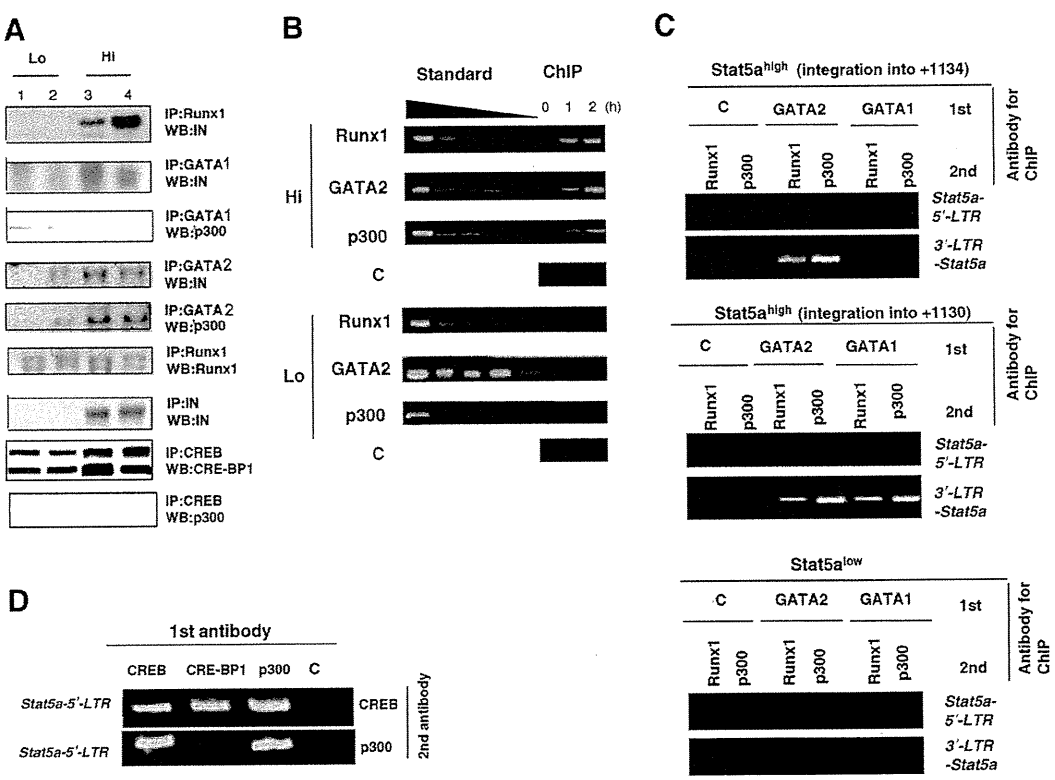

Figure 5. The IP of integrase (IN) complex and chromatin IP (ChIP) assays. Hi, Stat5a^{high} clones; Lo, Stat5a^{low} clones. **A:** The IP assay, lymphoma clone extracts. WB indicates Western blot. **Lanes 1** and **2:** Stat5a^{low} clones (integration sites, 1109 and 1115). **Lanes 3** and **4:** Stat5a^{high} clones (integration sites, 1126 and 1130). A photograph of WB using anti-CRE-BP1 revealed phosphorylated CRE-BP1 (upper band) and nonphosphorylated CRE-BP1. **B:** Reperformed ChIP-PCR assay. The chromatin preparation from 1.0×10^6 lymphoma cells was first immunoprecipitated with control and antibodies (first IP), and the immune complex was then eluted and reprecipitated with secondary antibodies (second IP). Primary and secondary antibodies used are shown. This also applies to the following figures. The upper photograph (*Stat5a-5′-LTR*) displays the results of PCR using primers between *Stat5a* and *Emv11* 5′-LTR. The lower photograph (*3′-LTR- Stat5a*) displays the results of PCR using primers between *Emv11* 3′-LTR and *Stat5a*. **C:** The ChIP-PCR assay. The photograph shows representative results of PCR using primers in the *Emv11* 3′-LTR and *Stat5a* third exon. The template DNA was extracted from chromatin preparations of 1.0×10^6 lymphoma cells and immunoprecipitated with antibodies against GATA2, Runx1, p300, or a normal rabbit IgG. Fivefold serial dilutions of total lymphoma DNA (standard) were amplified as an internal control of PCR using primers between −3346 and −2997 in the *Stat5a* gene (a and b, Stat5a^{high}; and c, Stat5a^{low}). **D:** Reperformed ChIP-PCR assay. The labels were identical to those in C.

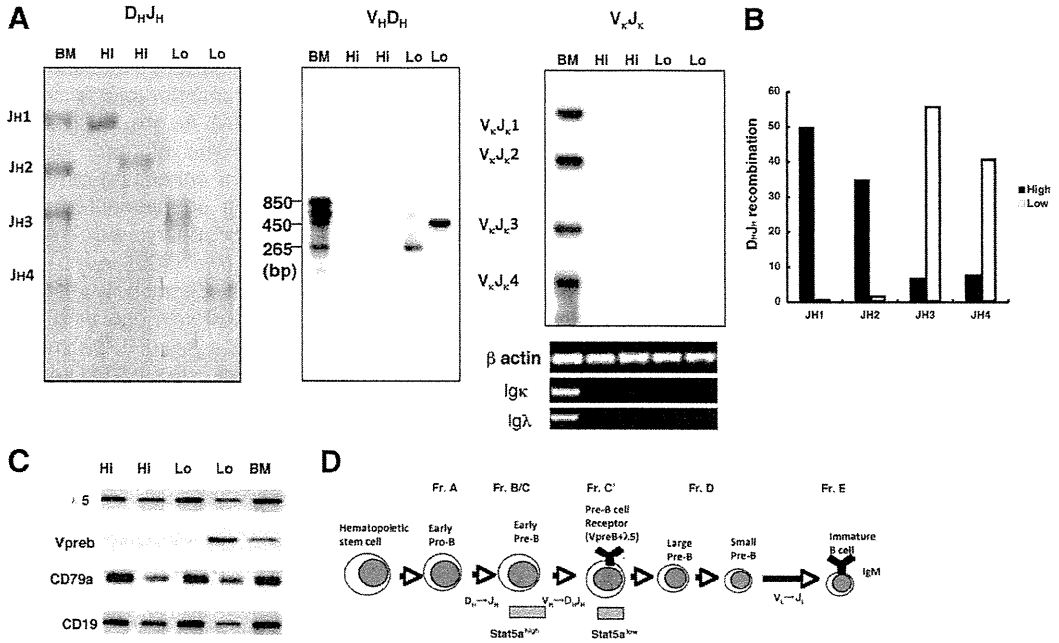

Figure 6. Development stages of pre–B lymphoma clones. **A:** Blots of D_HJ_H, IgH variable segment (V_H) and D_H, and VκDκ recombination. Hi indicates Stat5a^{high} clones; Lo, Stat5a^{low} clones; BM, pre–B cells of SL/Kh mice without the somatic *Emv11* integration 3 weeks after birth. **Lower:** Results of the RT-PCR assay for Igκ and Igλ expression. **B:** Type of D_HJ_H recombination in the clones. Percentages of the dominant type in individual Stat5a^{high} and Stat5a^{low} clones are presented. **C:** Results of RT-PCR for pre–B-cell receptor and other phenotypic markers. Hi indicates Stat5a^{high} clones (with integration into 1130); Lo, Stat5a^{low} clones (with integration into 1138); BM, pro–B cells obtained from SL/Kh mice 3 weeks after birth. **D:** Hardy's classification of Stat5a^{high} clones and Stat5a^{low} clones. Fr represents fraction. The stages of the B-cell lineage are shown.

and GATA2-p300 complexes in Stat5a^{high} clones (Figure 5C, a and b), whereas the *Emv11*-3′-LTR-*Stat5a* segment was not coimmunoprecipitated with these complexes (Figure 5C, c). In addition, the *Emv11*-3′-LTR-*Stat5a* segment from the clone with *Emv11* integration into 1130 was coimmunoprecipitated with GATA1-Runx1 and GATA1-p300 complexes (Figure 5C, b). Thus, the GATA-1 site could be referred to as a composite site that was formed *de novo* by the integration event. In addition, the *Stat5a-Emv11-5′*-LTR fusion segment was coimmunoprecipitated with the CRE-BP1-CREB and p300-CREB complexes (Figure 5D).

Integration Site Affects Maturation of Host Pro–B Lymphoma Cells

We investigated the integration site to determine its influence on the phenotype of host lymphoma clones. The STAT5A is involved in the malignant transformation of pro– and pre–B phenotypes.[17] The Stat5a^{high} clones completed IgH D_HJ_H recombination but not IgH variable segment–D_H recombination; on the other hand, Stat5a^{low} clones completed both D_HJ_H and IgH variable segment–D_H recombination. In both types of clones, Ig light chain recombination in Ig κ and Ig λ was not detected (Figure 6A). In the Stat5a^{high} clones, distal segments J_H1 and J_H2 were dominantly selected in D_HJ_H recombination, whereas in the Stat5a^{low} clones, proximal segments J_H3 and J_H4 were dominantly selected (significant findings) (Figure 6B). In addition, RT-PCR assays revealed that Stat5a^{high} clones were high for λ5 but low for *Vpreb*, surrogate light chain components of pre–B-cell receptor; in contrast, Stat5a^{low} clones were constitutively high for both λ5 and *Vpreb*. However, *Vpreb* expression was not constitutively high in Stat5a^{low} clones (Figure 6C). In summary, according to the murine B-cell classification of Hardy et al,[18] the Stat5a^{high} clones belonged to fraction B/C (pro– to early pre–B cells) and were more immature than other Stat5a^{low} clones that belonged to fraction C′ (pre–B cells) (Figure 6D). Thus, different integration sites of MLV influenced the development stage of the host cells.

Stimulation by IL-7 Receptor Suppressed Ig Light Chain Recombination in the Stat5a^{high} Lymphoma Clones

We then analyzed the effect of IL-7, one of the activation factors of signaling pathways that recruit STAT5A, on the development of Stat5a^{high} clones. The clones were first incubated for 24 hours in a medium without IL-7 to suppress intrinsic stimulation by IL-7 responses. Then, the knockdown of *Stat5a* was achieved by transfection of RNAi into the clones, performed with or without IL-7 for 120 hours. The knockdown was confirmed by Western blot analysis using an antibody toward STAT5A (Figure 7A).

After transfection, the expression of Ig κ and Ig λ was investigated by measuring the intensity of the Western blot. After incubation for 120 hours without *Stat5a* knockdown, IL-7 in the culture medium effectively suppressed Ig κ and Ig λ expression in Stat5a^{high} lymphoma clones (i versus ii); in contrast, the suppression was not evident in

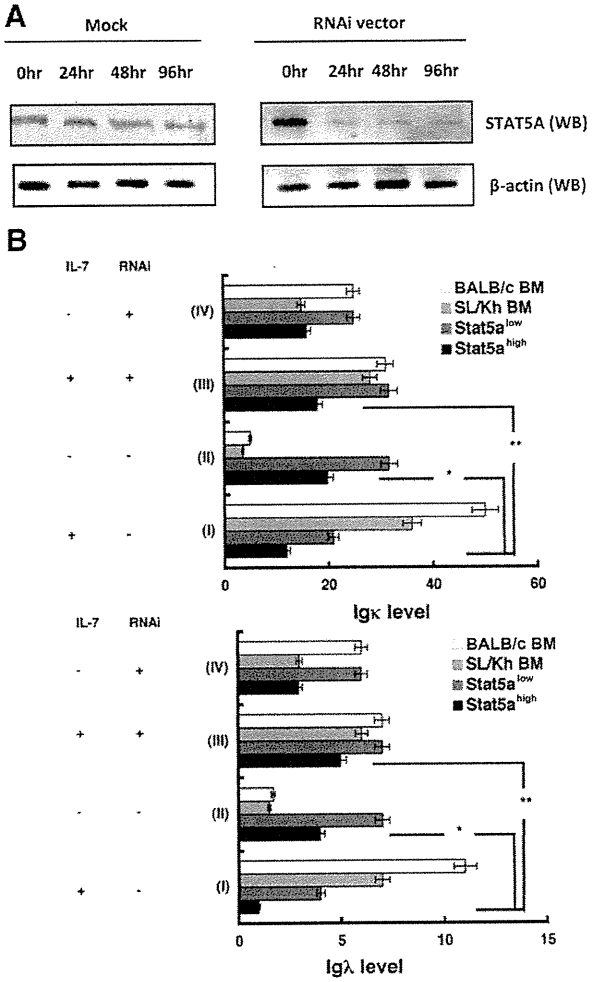

Figure 7. Arrest of Ig light chain (IgL) recombination in the Stat5a^{high} lymphoma clones supplemented with IL-7. **A:** Western blots (WBs) of the Stat5a^{high} clone with knockdown using control or both *Stat5a*- and *Stat5b*-RNAi with 50 ng/ml IL-7 or without IL-7 added. β-Actin was used as the control. **B:** The relative fluorescence intensity of Ig κ and Ig λ. For Stat5a^{high}, integration sites were 1124, 1126, 1130 (three clones), and 1134; Stat5a^{low}, integration sites were 1100, 1102, 1109, 1113, 1115, and 1138; SL/Kh BM, sorted normal pro–B cells without *Emv11* integration into *Stat5a* in the BM of SL/Kh mice; BALB/c BM, sorted control pro–B cells in the BM of BALB/c mice; + and −, presence and absence of 50 ng/ml IL-7 in the incubation medium for 96 hours, respectively. **Top: i** versus **ii**, $^{*}P = 0.034$ ($n = 5$); and **i** versus **iii**, $^{**}P = 0.041$ ($n = 5$). **Bottom: i** versus **ii**, $^{*}P = 0.013$; and **i** versus **iii**, $^{**}P = 0.023$. Assays were independently performed five times using four Stat5a^{high} clones and four Stat5a^{low} clones. Luciferase activity was assessed using Student's *t*-test.

Stat5a^{low} lymphoma clones (Figure 7). Incubation for 120 hours of the knockdown of *Stat5a* with IL-7 resulted in Ig κ and Ig λ expression in Stat5a^{high} lymphoma clones (i versus iii). Thus, the suppressive effect of IL-7 on Ig κ and Ig λ expression was exclusively evident in Stat5a^{high} lymphoma clones, indicating that the suppressive effect was dependent on the expression level of *Stat5a*.

IL-7 Receptor Stimulation Suppressed Apoptosis in the Stat5a^{high} Lymphoma Clones

There was an antiapoptotic effect of high expression of *Stat5a*. The clones were first incubated for 24 hours in a medium without IL-7 to suppress intrinsic stimulation by IL-7 responses. Next, supplying 50-ng/ml IL-7 during incubation resulted in significant up-regulation of the expression of Bcl-xL, an antiapoptotic protein, in the Stat5a^{high} clones (Figure 8A). As previously reported, the *bcl-xL* gene carries a gamma interferon activation site element in the promoter for enhancing dimeric STAT5A binding.[19] When IL-7 was supplemented, the relative densities of Bcl-xL and phosphorylated STAT5A closely correlated with each other ($P < 0.001$, $n = 5$) (Figure 8B).

Next, we performed an electromobility shift assay to investigate whether STAT5A protein can bind to the *bclxL* gene promoter after various levels of IL-7 stimulation using oligonucleotides corresponding to the STAT5A-binding motif on the murine *bcl-xL* gene promoter as a probe. After the addition of an antibody to the nuclear extracts, supershifts of the DNA binding complex were observed in an IL-7 dose-dependent manner (Figure 8C).

To confirm the effect of the increase in *bclxL* gene expression, the ratio of annexin V–positive apoptotic cells in the lymphoma clones was determined, with or without the addition of a cytokine supplement during the incubation. The results revealed that apoptotic cells were significantly less prevalent in Stat5a^{high} clones incubated with IL-7 (Figure 8D).

Discussion

The obtained data were used to construct a model to demonstrate why integration of a proviral genome into the specified location in the host sequence causes higher promoter activity and maturation arrest of the host cell (Figure 9). First, we found that Runx1, GATA2, and p300 bound to the 3′-LTR-*Stat5a* in the Stat5a^{high} clones (Figure 5, B and C). Next, we confirmed that CREB, CRE-BP1, and p300 bound to the 5′-LTR-*Stat5a* in the Stat5a^{high} clones (Figure 5D). This CREB protein has the potential to associate with CRE-BP1 and p300 in B cells and to control the transcription of the target gene. Therefore, CREB can be a scaffold for the recruitment of p300 on the LTR-*Stat5a* sequence DNA. Novel control of the CREB-dependent transcription of the target gene by a member of the regulator of G-protein signaling protein family in B cells has been reported.[20,21] The p300 increases target gene expression in several ways (ie, relaxing the chromatin structure at the gene promoter through its intrinsic histone-acetyltransferase activity and recruiting the general transcriptional machinery, including RNA polymerase II, to the promoter). In B cells, B-cell receptor linking induces histone lysine acetylation at the Bruton's tyrosine kinase promoter, correlating with marked recruitment of p300 to the locus.[22] Another recent study[23] reported that a paired box protein Pax5-mediated B-cell development was controlled by p300. Pax5 is a B-cell–specific activator protein that plays important roles in controlling the expression of lineage and differentiation stage–specific genes during B lymphopoiesis. Furthermore, p300 is a coactivator for transcription factor REL and is C terminally truncated in the human diffuse large B-cell lymphoma cell line.[24] Thus, p300 contributes to B-

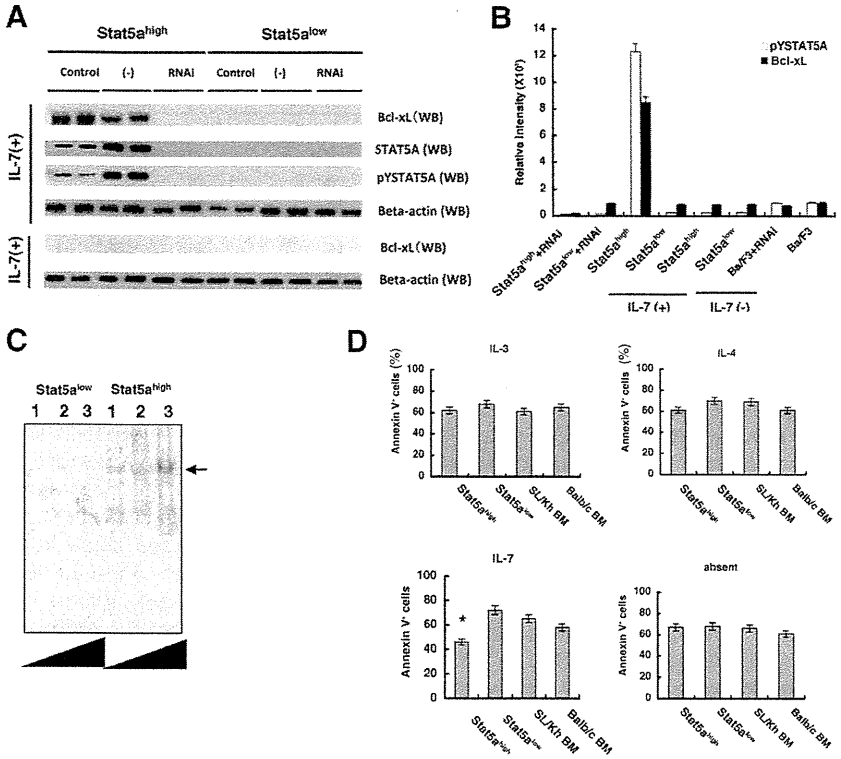

Figure 8. Expression of Bcl-xL in lymphoma clones. **A:** The RT-PCR assay of *bcl-xL* using Stat5a^{high} and Stat5a^{low} lymphoma clones. WB indicates Western blot. **B:** Relative density of the WBs for phosphorylated STAT5A (pYSTAT5A) and Bcl-xL. The density was measured with chemiluminator LumiVision. **C:** Identification of Stat5A binding by supershift analysis. **Lanes 1**, **2**, and **3:** Nuclear extracts of lymphoma cells stimulated with 0, 20, and 40 ng/mL of recombinant murine IL-7, respectively. The **arrow** highlights the supershift. **D:** Percentage of annexin V–positive cells in the population of lymphoma cells incubated with or without cytokines ($n = 5$, $^*P < 0.05$, Stat5a^{high} versus others).

cell development and lymphomagenesis. The histone-acetyltransferase activity of p300 modulates human T-lymphotropic virus-I LTR transcriptional activity.[25] Herein, we hypothesize that p300 bindings may promote the expression of MLV and the target *Stat5a*. Although there have been few reports regarding the relation of p300 with MLV LTR transcriptional activity, we suppose that direct p300 binding to the upstream sequence of the provirus or an indirect effect via association with CREB binding to the upstream sequence up-regulates the transcriptional activity; in addition, p300 binding to the downstream sequence may contribute to the transcriptional activity

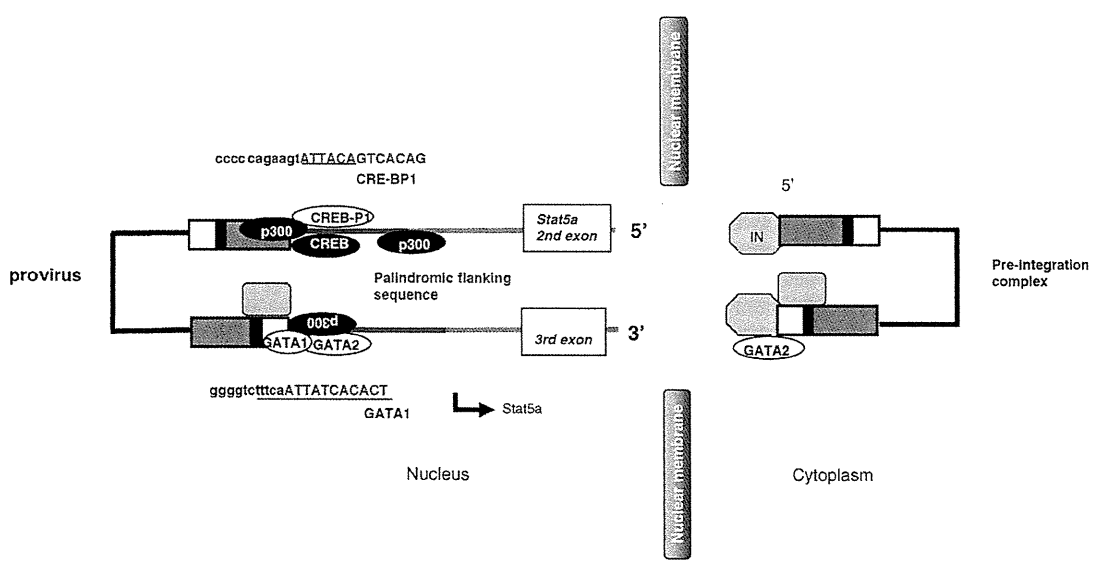

Figure 9. Model of the complex promoting transcription of the target gene. Transcription factor complexes on the LTR-*Stat5a* sequence. The provirus is integrated into 1130 and into another site. Transcription of LTR started from the RU5 element on the proviral genome. Lines by the sequence represent the CRE-BP1 and GATA1 motifs. The sequences next to the viral *Stat5a* segment display the motifs of p300, CREB, CRE-BP1, GATA2, Runx1, and GATA1. Lowercased letters represent MLV-LTR element sequences; and uppercased letters, *Stat5a* sequences. IN indicates integrase.

Table 3. MLV Integrations Near the Coding Region

Host gene located downstream of the integration site	Mouse chromosome		
	Size, bp	No.	Location
ATPase, H^+-transporting, V1 subunit G isoform 2	3,623 and 3,723	17	NT_039649
Fc-γ receptor	155,834	3	NT_39240
GRP1-binding protein GRSP1 (Frmd4b)	16,330	6	NT_039353.7
Myosin, heavy polypeptide 9, nonmuscle isoform 1	22,229	15	NT_039621.7
Similar to Gpd1l protein	5,189	5	NW_001030784.1
Similar to high-mobility group box 1	22,452	15	NT_039621.7
3-Hydroxyanthranilate-3,4-dioxygenase	292,004	17	NW_001030622.1
Testicular serine protease 1	7,060	1	NT_039170.7

downstream of *Stat5a* (Figure 2A, ii). This multiplier effect of p300 downstream and upstream of the provirus may contribute to a significant increase in the proviral promoter activity and the higher expression of *Stat5a*. A plausible regulation is that the palindromic sequence contributed to the stabilization of the relaxed chromatin by generation of a secondary structure, such as a cruciform or hairpin structure in the single-stranded DNA. Significantly, acetylation of HIV-1 integrase by p300 regulates viral integration.[26,27] Studamire and Goff[28] reported host proteins interacting with the Moloney murine leukemia virus integrase. In the future, other interacting proteins will be identified, and p300 may be among them.

When MLV is integrated into the most frequent integration site (ie, 1130), the *de novo* GATA1-binding motif appears in the provirus-host junctional sequence (Figure 5C). Indeed, the IP assay shown in Figure 5C indicates that GATA1 binds to the *Emv11* 3′-LTR-*Stat5a* segment. Thus, the proviral terminal sequence DNA connected to the host sequence DNA carries several potential transcription factor–binding motifs. The binding GATA1 may be controlled by acetylation by CRE-BP1.[29]

In the current study, a significant amount of integrase was unexpectedly observed in the lymphoma clones. The mean ± SD of 68 ± 17 nonclonal integration sites was identified in an examined clone by an inverse PCR method; the integration sites that are relatively close to the coding regions are listed in Table 3. These data suggested that MLV integration constitutively occurred in the lymphoma cells. In actuality, expression of ecotropic virus *Emv11* by neonatal injection of maternal resistance factor inhibits lymphomagenesis.[11] It is probable that MLV particles were provided by individual lymphoma cells and that the MLV reinfected neighboring lymphoma cells during tumor development, with translocation of integrase into the nucleus. This SL/Kh strain of mice possesses more than six copies of endogenous retroviruses in the germ line (Figure 1B). Six is a far higher number than that in other strains of mice, such as AKR.[12] A previous report[11] shows that two of these endogenous retroviruses have the potential to be transcribed into producing complete viral particles. In this study, we found three endogenous retroviruses other than *Emv11* (see Supplemental Table S1 at *http://ajp.amjpathol.org*). These endogenous retroviral transcriptional mechanisms and functions are not entirely understood, and further study will be required for consideration of a model in which integrase interacts with transcriptional factors in the host cells. Notably, Kitamura et al reported that human endogenous retrovirus K10 encodes a functional integrase.[30]

Our data clearly show that the *Emv11* integration site influences host phenotype via the maturation arrest of the *IgH* recombination. These influences by the integration site remain poorly understood, and insufficient attention has been paid to host phenotypic changes aside from *Emv11* tumorigenesis. However, as shown in the current study, the integration site can have variable effects on host phenotype via integration. Although our study is limited to *IgH* recombination in the presence of IL-7, the cell culture conditions may affect the host cell phenotype by the integration. In this model, we added evidence that STAT5A may contribute to the tumorigenesis of pre–B lymphoma/leukemia. In actuality, there have been reports[31,32] that mutations of Janus kinase 2, which phosphorylates STAT5, in acute lymphocytic leukemia are associated with Down's syndrome. Thus, the contribution of STAT5 to leukemogenesis has been commonly accepted. Our study model could be one of the models of lymphoblastic tumorigenesis.

The MLV vectors are essential tools for the generation of induced pluripotent stem cells. Nevertheless, the data presented herein provide significant information about the phenotypes of transgenic animals carrying the MLV vector. A minute difference between MLV integration sites can lead to large differences in host phenotype, suggesting that caution should be advised in monitoring integration sites when working with MLV vectors.

Acknowledgments

We thank Dr. Hiroshi Hiai (Kyoto University, Kyoto, Japan) for overview and critical advice regarding the manuscript; Dr Tasuku Honjo, Kyoto University, for critical advice regarding the manuscript; and Ms. H. Saito for providing technical assistance.

References

1. Hacein-Bey-Abina S, Von Kalle C, Schmidt M, McCormack MP, Wulffraat N, Leboulch P, Lim A, Osborne CS, Pawliuk R, Morillon E, Sorensen R, Forster A, Fraser P, Cohen JI, de Saint Basile G, Alexander I, Wintergerst U, Frebourg T, Aurias A, Stoppa-Lyonnet D, Romana S, Radford-Weiss I, Gross F, Valensi F, Delabesse E, Macintyre E, Sigaux F, Soulier J, Leiva LE, Wissler M, Prinz C, Rabbitts TH, LE Deist F, Fischer A, Cavazzana-Calvo M: LMO2-associated clonal

T cell proliferation in two patients after gene therapy for SCID-X1. Science 2003, 302:415–419
2. Nakagawa M, Koyanagi M, Tanabe K, Takahashi K, Ichisaka T, Aoi T, Okita K, Mochiduki Y, Takizawa N, Yamanaka S: Generation of induced pluripotent stem cells without Myc from mouse and human fibroblasts. Nature Biotechnol 2008, 26:101–106
3. Akagi K, Suzuki T, Stephens RM, Jenkins NA, Copeland NG: RTCGD: retroviral tagged cancer gene database. Nucleic Acids Res 2004, 32:D523–D527
4. Tsuruyama T, Nakamura T, Jin G, Ozeki M, Yamada Y, Hiai H: Constitutive activation of Stat5a by retrovirus integration in early pre-B lymphomas of SL/Kh strain mice. Proc Natl Acad Sci U S A 2002, 99:8253–8258
5. Matsumura I, Kitamura T, Wakao H, Tanaka H, Hashimoto K, Albanese C, Downward J, Pestell RG, Kanakura Y: Transcriptional regulation of the cyclin D1 promoter by STAT5: its involvement in cytokine-dependent growth of hematopoietic cells. EMBO J 1999, 18:1367–1377
6. Nosaka T, Kawashima T, Misawa K, Ikuta K, Mui AL, Kitamura T: STAT5 as a molecular regulator of proliferation differentiation and apoptosis in hematopoietic cells. EMBO J 1999, 17:4754–4765
7. Kirito K, Watanabe T, Sawada K, Endo H, Ozawa K, Komatsu N: Thrombopoietin regulates Bcl-xL gene expression through Stat5 and phosphatidylinositol 3-kinase activation pathways. J Biol Chem 2002, 277:8329–8337
8. Chowdhury D, Sen R: Stepwise activation of the immunoglobulin mu heavy chain gene locus. EMBO J 2000, 20:6394–6403
9. Sexl V, Piekorz R, Moriggl R, Rohrer J, Brown MP, Bunting KD, Rothammer K, Roussel MF, Ihle JN: Stat5a/b contribute to interleukin 7-induced B-cell precursor expansion but abl- and bcr/abl-induced transformation are independent of Stat5. Blood 2000, 96:2277–2283
10. Schwaller J, Parganas E, Wang D, Cain D, Aster JC, Williams IR, Lee CK, Gerthner R, Kitamura T, Frantsve J, Anastasiadou E, Loh ML, Levy DE, Ihle JN, Gilliland DG: Stat5 is essential for the myelo- and lymphoproliferative disease induced by TEL/JAK2. Mol Cell 2000, 6:693–704
11. Abujiang P, Yamada Y, Haller O, Kobayashi H, Kamoto T, Lu LM, Ogawa M, Ishimoto A, Katoh H, Kanehira K, Ikegami S, Fukumoto M, Hiai H: The origin of SL family mice. Lab Anim Sci 1996, 62:410–417
12. Mucenski ML, Bedigian HG, Shull MM, Copeland NG, Jenkins NA: Comparative molecular genetic analysis of lymphomas from six inbred mouse strains. J Virol 1988, 62:839–884
13. Pennycook JLMH, Marshall AJ, Wu GE: PCR assays for endogenous Ig gene rearrangement. Immunology Methods Manual, vol 1. Edited by I Lefkovits. San Diego, Academic Press, 1997, pp 564
14. Ye SK, Maki K, Kitamura T, Sunaga S, Akashi K, Domen J, Weissman IL, Honjo T, Ikuta K: Induction of germline transcription in the TCRγ locus by Stat5: implications for accessibility control by the IL-7 receptor. Immunity 1999, 11:213–223
15. Ishihara K, Satoh I, Nittoh T, Kanaya T, Okazaki H, Suzuki T, Koyama T, Sakamoto T, Ide T, Ohuchi K: Preparation of recombinant rat interleukin-5 by baculovirus expression system and analysis of its biological activities. Biochim Biophys Acta 1999, 1451:48–58
16. Shang Y, Hu X, DiRenzo J, Lazar MA, Brown M: Cofactor dynamics and sufficiency in estrogen receptor-regulated transcription. Cell 2000, 103:843–852
17. Santos SC, Lacronique V, Bouchaert I, Monni R, Bernard O, Gisselbrecht S, Gouilleux F: Constitutively active STAT5 variants induce growth and survival of hematopoietic cells through a PI 3-kinase/Akt dependent pathway. Oncogene 2001, 20:2080–2090
18. Hardy RR, Carmack CE, Shinton SA, Kemp JD, Hayakawa K: Resolution and characterization of pro-B and pre-pro-B cell stages in normal mouse bone marrow. J Exp Med 1991, 173:1213–1225
19. Socolovsky M, Fallon A, Wang S, Brugnara C, Lodish H: Fetal anemia and apoptosis of red cell progenitors in Stat5a-/-5b-/- mice: a direct role for Stat5 in Bcl-xL induction. Cell 1999, 98:181–191
20. Vo N, Goodman RH: CREB-binding protein and p300 in transcriptional regulation. J Biol Chem 2001, 276:13505–13508
21. Xie Z, Geiger TR, Johnson EN, Nyborg JK, Druey KM: RGS13 acts as a nuclear repressor of CREB. Mol Cell 2008, 31:660–670
22. Spiegelman BM, Heinrich R: Biological control through regulated transcriptional coactivators. Cell 2004, 119:157–167
23. Lee IS, Choi WH, Kim JY, Jeong JY, Kim MJ, Nam JH, Kim JH, Seo SB, Pak JH: Transcriptional regulation of the murine 1-cys peroxiredoxin gene by the B cell-specific activator protein, Pax5. J Cell Biochem 2008, 104:465–476
24. Garbati MR, Alço G, Gilmore TD: Histone acetyltransferase p300 is a coactivator for transcription factor REL and is C-terminally truncated in the human diffuse large B-cell lymphoma cell line RC-K8. Cancer Lett 2010, 291:237–245
25. Michael B, Nair AM, Datta A, Hiraragi H, Ratner L, Lairmore MD: Histone acetyltransferase (HAT) activity of p300 modulates human T lymphotropic virus type 1 p30II-mediated repression of LTR transcriptional activity. Virology 2006, 354:225–239
26. Cereseto A, Manganaro L, Gutierrez MI, Terreni M, Fittipaldi A, Lusic M, Marcello A, Giacca M: Acetylation of HIV-1 integrase by p300 regulates viral integration. EMBO J 2005, 24:3070–3081
27. Raghavendra NK, Shkriabai N, Graham RLJ, Hess S, Kvaratskhelia M, Wu L: Identification of host proteins associated with HIV-1 preintegration complexes isolated from infected CD4+ cells. Retrovirology 2010, 7:66
28. Studamire B, Goff SP: Host proteins interacting with the Moloney murine leukemia virus integrase: multiple transcriptional regulators and chromatin binding factors. Retrovirology 2008, 5:48
29. Hung HL, Lau J, Kim AY, Weiss MJ, Blobel GA: CREB binding protein acetylates hematopoietic transcription factor GATA-1 at functionally important sites. Mol Cell Biol 1999, 19:3496–3505
30. Kitamura Y, Ayakawa T, Ishikawa T, Kanda T, Yoshiike K: Human endogenous retrovirus K10 encodes a functional integrase. J Virol 1996, 70:3302–3306
31. Bercovich D, Ganmore I, Scott LM, Wainreb G, Birger Y, Elimelech A, Shochat C, Cazzaniga G, Biondi A, Basso G, Cario G, Schrappe M, Stanulla M, Strehl S, Haas OA, Mann G, Binder V, Borkhardt A, Kempski H, Trka J, Bielorei B, Avigad S, Stark B, Smith O, Dastugue N, Bourquin JP, Tal NB, Green AR, Izraeli S: Mutations of JAK2 in acute lymphoblastic leukaemias associated with Down's syndrome. Lancet 2008, 372:1484–1492
32. Kearney L, Gonzalez De Castro D, Yeung J, Procter J, Horsley SW, Eguchi-Ishimae M, Bateman CM, Anderson K, Chaplin T, Young BD, Harrison CJ, Kempski H, So CW, Ford AM, Greaves M: Specific JAK2 mutation (JAK2R683) and multiple gene deletions in Down syndrome acute lymphoblastic leukemia. Blood 2009, 113:646–648

京都大学大学院医学研究科人間健康科学系専攻紀要
健康科学　第7巻　2011

原　著

Pyothorax-associated Lymphoma : Loss of Epstein-Barr Virus Nuclear Antigen-3B Protein Expression as a Result of Mismatch Repair Phenotypes

Tetsuya TAKAKUWA

Abstracts : Pyothorax-associated lymphoma (PAL) is an EBV-associated lymphoma, which develops in the pleural cavity of immunocompetent patients with an over-20-year history of pyothorax. PAL tumor cells taken from a 72-year-old man revealed having mismatch repair (MMR) phenotype and expression of all Epstein-Barr virus latent genes except EBNA-3B. EBNA-3B gene in the derived cell line had frameshift mutation in mononucleotide repeats, indicating that EBNA-3B was the target for the MMR phenotype. Because EBNA-3B works as target antigens for host cytotoxic T-lymphocyte (CTL) responses via two HLA-A11-restricted epitopes, loss of EBNA-3B expression may contribute for PAL cells to escape from host immune surveillance in the present case.

Key words : Pyothorax-associated lymphoma, Epstein-Barr virus, EBNA-3B, Mismatch repair phenotypes

Introduction

Malignant lymphoma frequently develops in the pleural cavity of patients with over 20-year history of pyothorax[1]. This tumor stand as a distinct clinicopathologic entity, thus the term pyothorax-associated lymphoma (PAL) has been proposed for this type of tumor[2]. PAL is now listed as a distinct disease entity in the recent World Health Organization Classification of tumors[3]. PAL is non-Hodgkin lymphoma, mostly diffuse large B-cell lymphoma (DLBCL), which is strongly associated with Epstein-Barr virus (EBV) infection.

Previous study on a relatively small number of PAL cases reported the Latency (Lat) III pattern of EBV infection at protein level, i.e. the tumor cells express all 9 latent genes[4]. Whereas, we recently demonstrated that the EBV latency pattern in PAL was various among cases[5]. Latent infection antigens of EBV, including EBV nuclear antigens (EBNAs) and latent membrane proteins, are expressed in latently infected and immortalized B cells but they work as target antigens for host cytotoxic T-lymphocyte (CTL) responses in a HLA class I-restricted manner[6,7]. Among these latent antigens, the immunodominant CTL epitopes in EBNA-3B (EBNA-3B 399-408 and EBNA-3B 416-424) are well characterized. The major cytolytic activity of the host CTL is induced via two HLA-A11-restricted epitopes in the viral EBNA-3B antigen[6,7].

Usually, there are no clinical findings suggesting the presence of immune dysfunction in patients with PAL[1,2]. Therefore some mechanism for PAL cells to escape from host immune surveillance must be present. Production of immunosuppressive cytokine IL-10 by PAL cells, decreased of expression of HLA class I molecules in PAL cells, or mutation of CTL-epitope in EBNA3B might be involved in the escape of PAL cells from CTL[8-10].

We have established several cell lines from PAL tissues[11]; among them one line (OPL-3) with Lat III pattern of latent gene expression did not express EBNA-3B protein. Sequencing analysis revealed frameshift mutations in mononucleotide repeats within EBNA-3B gene, which generates premature stop codon, thus abolish EBNA-3B protein expression. In addition to reduction of HLA class 1 molecules, loss of the EBNA-3B expression may contribute to PAL cells to escape from host immune surveillance. The host tumor cells were mismatch repair (MMR) phenotype, which may cause in mutations of EBNA-3B genes.

Case report

A 72-year-old man was admitted to National Kinki-Chuou Hospital with left chest pain. He had suffered from pulmonary tuberculosis in the left lung and received an artificial pneumothorax when he was 22 years old. Computed tomographic (CT) scan on admission of this time revealed the masses in the left pleural cavity and diaphragm,

Human Health Science, Graduate School of Medicine, Kyoto University
Sakyo-ku Shogoin Kawahara-cyo 53, Kyoto 606-8507, Japan
受稿日　2011年9月15日
受理日　2012年1月19日

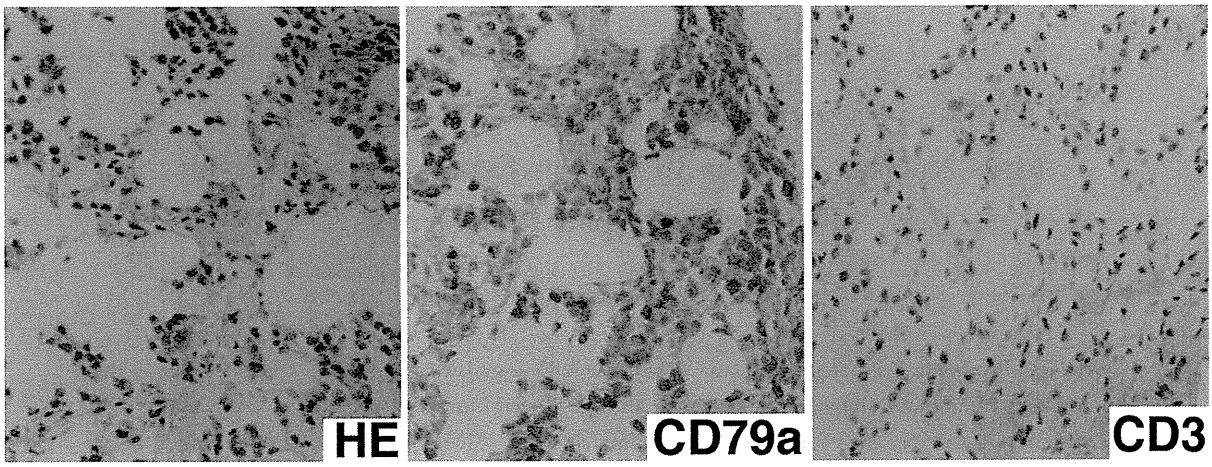

Fig. 1 Aspiration biopsy from the pleural cavity revealed a monomorphous proliferation of large lymphoid cells in the collagens and fat tissues (HE). Immunohistochemistry revealed that these cells were positive for CD79a and negative for CD3, thus diagnosed as diffuse large lymphoma of B-cell type. Few intermingling small lymphocytes were observed.

which were affected by pyothorax. Aspiration biopsy from the pleura revealed monomorphic proliferation of large lymphoid cells in the collagens and fat tissues (Fig. 1). Immunohistochemistry revealed that most proliferating cells were positive for CD20 and CD79a, and negative for CD3, thus diagnosed as diffuse large lymphoma of B-cell type.

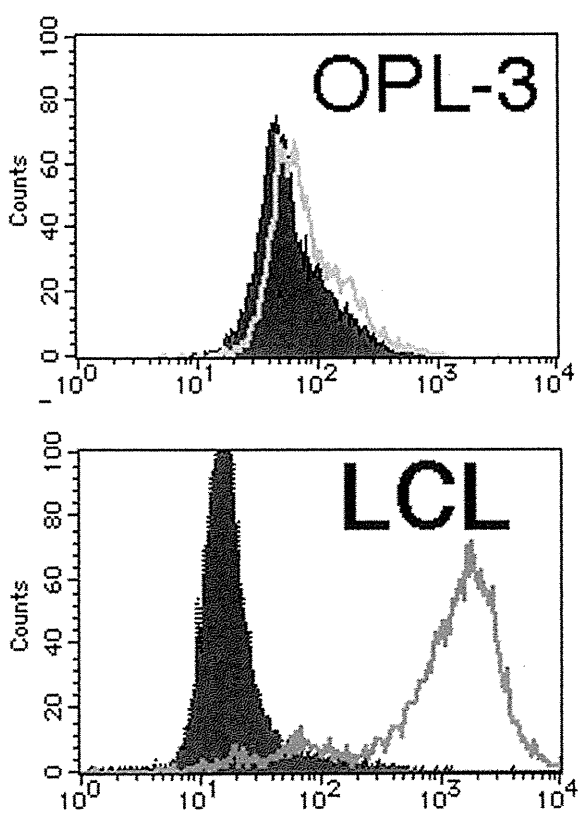

Fig. 2 Flow-cytometric analyses for expression of HLA class I antigens in PAL cell lines OPL-3 and EBV infected peripheral B lymphocytes (lymphoblastoid cell line ; LCL). Cells were incubated with HLA class I monoclonal antibody (white) or with control antibodies (shaded), incubated with FITC-labeled second antibodies, and analyzed with a flow-cytometry.

As for EBV gene expression, both LMP-1 and EBNA-2 were positive in immunohistochemistry. A cell line was established from a part of the sample with informed consent in accordance with the Declaration of Helsinki[11]. HLA-A allele of the patient was A2/A11 (data not shown). Flow-cytometric analyses of the cell line revealed slightly reduced, but definite expression of HLA class I molecule (Fig. 2). Radiographic examination including abdominal CT, brain magnetic resonance imaging, and Gallium scintigraphy together with bone marrow biopsy revealed metastasis in the spleen. Combined two courses of chemotherapy (cyclophosphamide, doxorubicin, vincristine, and prednisolone) and 50 Gy of radiation therapy were started, but he died of disease 30 months after admission. Autopsy was not performed.

Materials and Methods

1. HLA-A allotyping and flow-cytometric analysis for HLA class I

Low-resolution HLA-A locus-specific PCR typing of the patient was performed using HLA-A locus sequence-specific primers combinations in PCR amplification of genomic DNA as described previously[9]. Flow-cytometric analysis for expression of HLA class I molecule in the cell lines was done.

2. RT-PCR analysis for detection of EBV latent gene expression

Total RNA was extracted from the samples with the TRIzol reagent (Invitrogen, Inc., Rockville, MD) according to the manufacturer's instructions. Five μg of total RNA were reverse-transcribed by random hexamer priming using the Superscript first strand synthesis system (Invitrogen). Primer pairs were designed to distinguish different EBNA-1 promoter usage from each other, and to detect EBNA-2 and

EBNA-3B transcripts as described previously[5,12].

3. Detection of mutations

Long-distance PCR was performed to amplify the whole EBNA-3B gene. After electrophoresis on 1.0% agarose gel, DNA fragments were excised and purified using the Wizard SV gel extraction kit (Promega Co., Madison, WI). The purified DNA was used as template for PCR, and the products were directly sequenced with appropriate primers.

4. Western blotting

Western blotting was carried out as described previously[13]. Briefly, whole cells were lyzed in 1 x sample buffer, separated with 10% SDS-PAGE, and then blotted to polyvinylidene difluoride membrane using a wet-blotting apparatus. Anti-LMP-1 and -EBNA-2 antibodies were purchased from DAKO (Glostrup, Denmark), and anti-EBNA-3B antibody from Exalpha Biologicals (Boston, MA). Anti-actin antibody (Sigma, St. Louis, MO) was used as control. Signals were visualized with ECL plus Chemiluminescent reagents (GE Healthcare Bio-Sciences Corp., Piscataway, NJ).

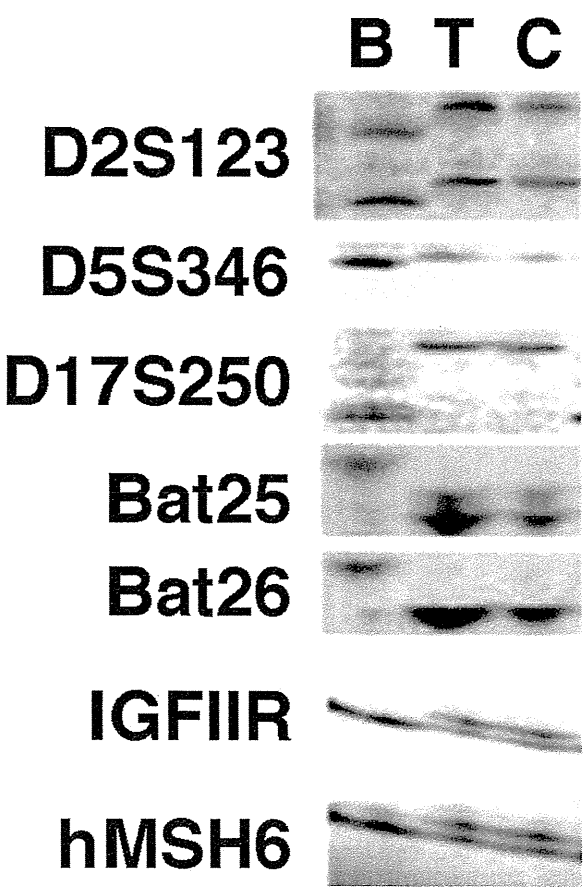

Fig. 3 According to the International Workshop on MSI and RER phenotypes in Cancer Detection and Familial Predisposition, five microsatellite repeats, D2S123, D5S346, D17S250, BAT25, and BAT26 were analyzed in OPL-3. MMR-target genes such as IGFIIR and hMSH6 were mutated. PCR products from established cell line (C), tumor (T) and corresponding peripheral blood leukocytes (B).

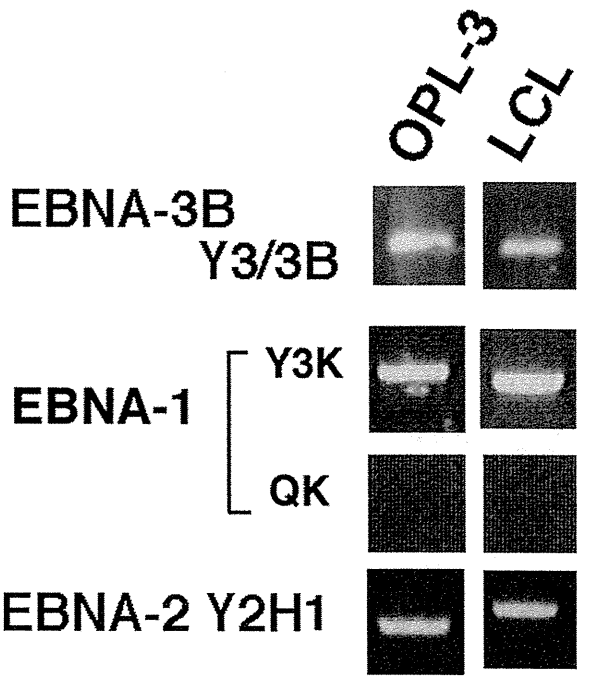

Fig. 4 Analysis of EBNA-1 promoter usage and expression of EBNA-2, and -3B transcripts in OPL-3. Products were visualized on agarose gels stained with ethidium bromide.

Results

The cell line (OPL-3) established from the patient was an immunophenotype of B cell and similar to that of the original biopsy specimen (i.e. positive for CD20, CD30 and CD79a, and negative for CD3, CD4, CD5, CD7, and CD8), which were confirmed with three different subclones. Terminal repeat of fusion of EBV in lymphoma cells was monoclonal pattern. Karyotype was complex with numerous structural and numerical abnormalities. Disruption of the MMR system, as revealed by Microsatellite Instability (MSI) was found (Fig. 3)[11]. According to the International Workshop on MSI and RER phenotypes in Cancer Detection and Familial Predisposition[14], four of five microsatellite repeats were positive. MMR target genes such as *IGFIIR* and *hMSH6* were also mutated. Promoter usage of EBNA-1 was Lat III pattern in OPL-3 (Fig. 4). LMP-1, EBNA-2, and EBNA-3B were also expressed as expected. LMP-1 and EBNA-2 proteins were expressed as well, whereas, EBNA-3B protein was not detected by Western Blotting analysis (Fig. 5).

Sequencing analysis of EBNA-3B in OPL-3 and peripheral blood leukocytes from the patient was performed. Compared with EBV genome in the strain B95-8, (Gene Acc V01555.2), more than 10 polymorphisms were observed in EBNA-3B from both OPL-3 and

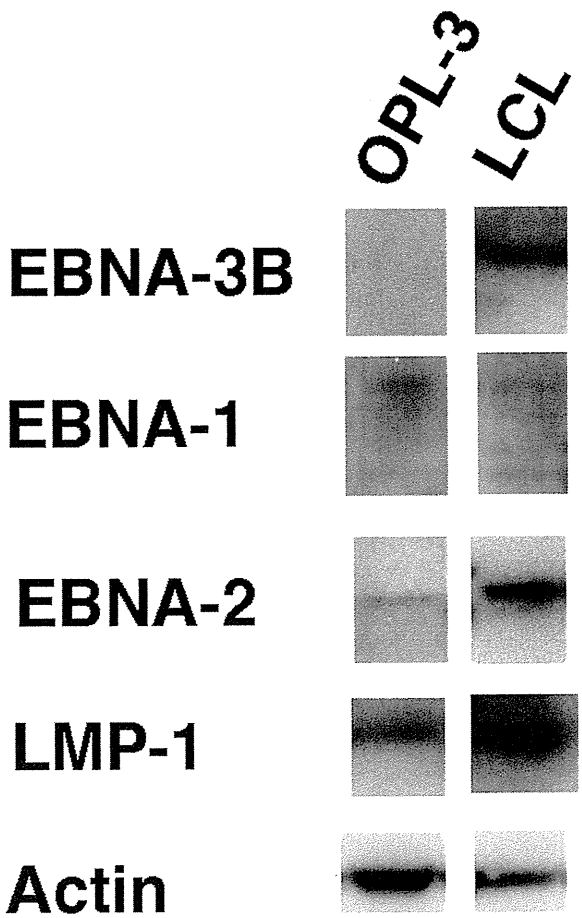

Fig. 5 Latent gene protein expression in PAL cell lines by Western blotting. Expression of EBNA-3B was not detected in OPL-3.

peripheral blood leukocytes (data not shown). Frameshift mutation at mononucleotide tracts from nucleotide 96007 to 96013 in OPL-3, which generates premature stop codon, was observed in OPL-3 but not in the peripheral blood leukocytes (Fig. 6).

Change in mononucleotide repeat lengths was not observed in other EBV latent genes including, LMP-1 (poly C7 ; nt number 5804–5810 in B95-8), EBNA-2 (poly C8 ; nt number 48696–48703), EBNA-3A (poly C7 ; nt number 94177–94183, nt number 94697–94703), EBNA-3B (poly A7 ; nt number 95887–95893, poly G7 ; nt number 95387–95393, nt number 95999–96005, number 98075–98081), EBNA-3C (poly C7 ; nt number 100738–100744), EBNA-1 (poly G7 ; nt number 107026–107032) as well as OriP regions (poly A8 ; nt number 8339–8346, poly C8 ; nt number 9439–9446) (data not shown).

Discussion

PAL is an EBV-associated lymphoma, which develops in patients with over 20 year-history of chronic pyothorax and with no evidence of immune dysfunction[1,2]. Because most PAL expresses full range of EBV latent genes, escape mechanisms from host CTL should work in PAL[4–7]. Indeed, OPL-3 showed the Lat III pattern of EBV latent gene expression and expressed HLA-A11. However, histologic examination of biopsy sample did not reveal the

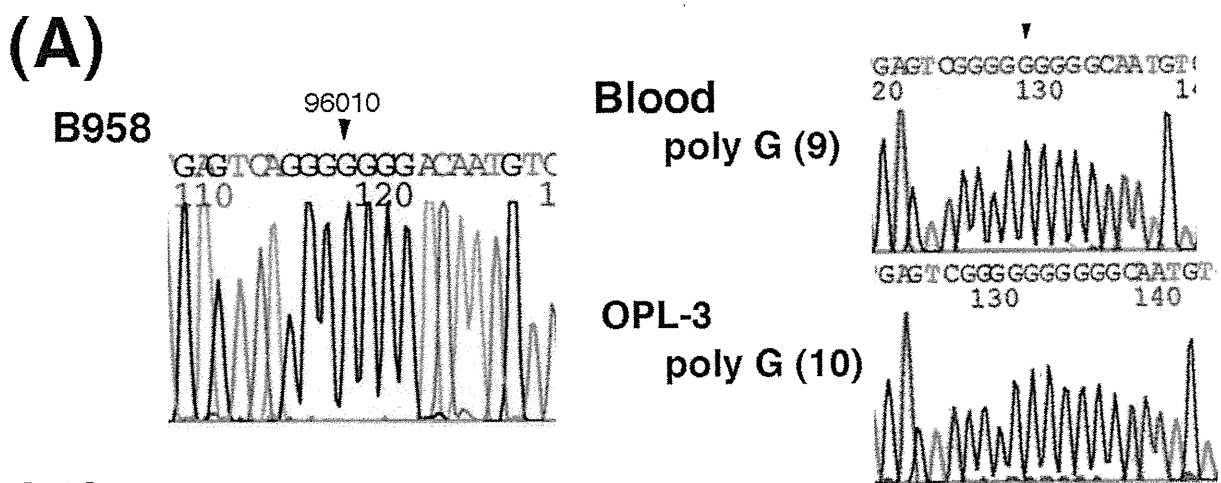

(B)

```
                    576          585          594          603          612          621
                    --- --- --- --- --- --- --- --- --- --- --- --- --- --- --- --- --- --- --- ---
B958        TTT GAG TCA GGG GGG GAC AAT GTC CAC CCG GTC CTT GTG ACT GCT ACG CTA GGA TGT GAT
polyG(9)    TTT GAG TCg GGG GGG GgA AAT GTC CAC CCG GTC CTT GTG ACT GCT ACG CTA GGA TGT GAT
polyG(10)   TTT GAG TCg GGG GGG Ggg CAA TGT CCA CCC GGT CCT TGT GAC TGC TAC GCT AGG ATG TGA

B958        Phe Glu Ser Gly Gly Asp Asn Val His Pro Val Leu Val Thr Ala Thr Leu Gly Cys Asp
polyG(9)    Phe Glu Ser Gly Gly Gly Asn Val His Pro Val Leu Val Thr Ala Thr Leu Gly Cys Asp
polyG(10)   Phe Glu Ser Gly Gly Gly Gln Cys Pro Pro Gly Pro Cys Asp Cys Tyr Ala Arg Met ***
```

Fig. 6 Sequencing of EBNA-3B gene containing at mononucleotide tracts from nucleotide 96007 to 96013 (A) and predicted amino acid sequences in OPL-3 (B). Frameshift mutation was observed in OPL-3, which gnerate premature stop codon. No frame shift mutations were observed in peripheral blood leukocytes. B95-8 sequence was shown as comparison.

findings suggestive of CTL response against the proliferating PAL cells, i.e., infiltration of T lymphocytes.

EBNA-3B protein was not expressed in OPL-3. The sequencing analysis revealed the frameshift mutations within EBNA-3B gene, which might result in loss of the EBNA-3B protein. The mutations were insertions within mononucleotide repeats, which are frequently observed in cells with MMR phenotypes. In the previous report[11], we demonstrated that OPL-3 had MMR phenotypes and MMR-target genes such as IGFIIR and hMSH6 was mutated. Because EBV replication is synchronized with host cell division using the host replication system, the simple repeat sequences in EBV genome might also be the target in the host with MMR phenotype. EBV genome contains many mononucleotide repeats. In the present study the insertion G was observed in only EBNA-3B gene in OPL-3. Further in vitro and *in vivo* study may be necessary whether loss of EBNA-3B may be growth advantage or not.

MMR type is rare in non-Hodgkin lymphoma except for immunodeficiency-related lymphoma such as HIV infection-related lymphomas and posttransplant lymphoproliferative disorders[15]. Immunotherapy employing antigen-specific T cells for treatment of human malignancies is becoming popular. EBNA-3B epitope is one of the candidates for the virus-specific CTL therapy in fatal lymphoproliferative diseases. Gottschalk et al reported a case in which CTL therapy to fatal lymphoproliferative disease resulted in the selection of clone with EBNA-3B deletion[16]. It is possible that EBNA-3B deletion clone might be selected in such lymphomas as same mechanism as observed in the present case.

The present case suggests that not only host genome but also infected EBV genome could be targets for mutations in cells with MMR phenotype. Resultant loss of latent gene EBNA-3B expression provides an advantage for tumor growth via escape from host CTL responses. This seems to be one of the mechanisms how PAL cells avoid from CTL response. It is interesting to know whether other EBV-related lymphomas have deficiency in EBNA-3B expression.

References

1) Nakatsuka S, Yao M, Hoshida Y, Yamamoto S, Iuchi K, Aozasa K : Pyothorax-associated lymphoma : a review of 106 cases. J Clin Oncol, 2003 ; 20 : 4255-4260
2) Iuchi K, Aozasa K, Yamamoto S, et al : Non-Hodgkin's lymphoma of the pleural cavity developing from long-standing pyothorax. Summary of clinical and pathological findings in thirty-seven cases. Jpn J Clin Oncol, 1989 ; 19 : 249-257
3) Banks PM, Harris NL, Warnke RA, Gaulard Ph : Lymphomas. In : Travis WD, Brambilla E, Mueller-Hermelink HK, Harris CC, eds. World Health Organization Classification of Tumors : Pathology and Genetics of tumors of the Lung, Pleura, Thymus and Heart. Lyon : IARC Press, 2004 : 137-140
4) Fukayama M, Ibuka T, Hayashi Y, Ooba T, Koike M, Mizutani S : Epstein-Barr virus in pyothorax-associated pleural lymphoma. Am J Pathol, 1993 ; 143 : 1044-1049
5) Takakuwa T, Ham MF, Luo WJ, Nakatsuka S, Daibata M, Aozasa K : Loss of expression of Epstein-Barr virus nuclear antigen-2 correlates with a poor prognosis in cases of pyothorax-associated lymphoma. Int J Cancer, 2006 ; 118 : 2782-2789
6) de Campos-Lima PO, Levitsky V, Brooks J, et al : T cell responses and virus evolution : loss of HLA A11-restricted CTL epitopes in Epstein-Barr virus isolates from highly A11-positive populations by selective mutation of anchor residues. J Exp Med, 1994 ; 179 : 1297-1305
7) Rickinson AB, Moss DJ : Human cytotoxic T lymphocyte responses to Epstein-Barr virus infection. Annu Rev Immunol, 1997 ; 15 : 405-431
8) Kanno H, Nakatsuka S, Iuchi K, Aozasa K : Sequences of cytotoxic T-lymphocyte epitopes in the Epstein-Barr virus (EBV) nuclear antigen-3B gene in a Japanese population with or without EBV-positive lymphoid malignancies. Int J Cancer, 2000 ; 88 : 626-632
9) Kanno H, Ohsawa M, Hashimoto M, Iuchi K, Nakajima Y, Aozasa K : HLA-A alleles of patients with pyothorax-associated lymphoma : anti-Epstein-Barr virus (EBV) host immune responses during the development of EBV latent antigen-positive lymphomas. Int J Cancer, 1999 ; 82 :630-634
10) Kanno H, Naka N, Yasunaga Y, et al : Production of the immunosuppressive cytokine interleukin-10 by Epstein-Barr virus expressing pyothorax-associated lymphoma : possible role in the development of overt lymphoma in immunocompetent hosts. Am J Pathol, 1997 ; 150 : 349-357
11) Takakuwa T, Luo WJ, Ham MF, Mizuki M, Iuchi K, Aozasa K : Establishment and characterization of unique cell lines derived from pyothorax-associated lymphoma which develops in long-standing pyothorax and is strongly associated with Epstein-Barr virus infection. Cancer Sci, 2003 ; 94 : 858-863
12) Oudejans JJ, van den Brule AJ, Jiwa NM, et al : BHRF1, the Epstein-Barr virus (EBV) homologue of the BCL-2 protooncogene, is transcribed in EBV-associated B-cell lymphomas and in reactive lymphocytes. Blood, 1995 ; 86: 1893-1902
13) Liu A, Takakuwa T, Fujita S, et al : Alterations of DNA damage-response genes ATM and ATR in pyothorax-associated lymphoma. Lab Invest, 2005 ; 85 : 436-446
14) Boland CR, Thibodeau SN, Hamilton SR, et al : A National Cancer Institute Workshop on Microsatellite Instability for cancer detection and familial predisposition : development of international criteria for the determination of microsatellite instability in colorectal cancer. Cancer Res, 1998 ; 58 : 5248-5257
15) Duval A, Raphael M, Brennetot C, et al : The mutator pathway is a feature of immunodeficiency-related lymphomas. Proc Natl Acad Sci USA, 2004 ; 101 : 5002-5007

16) Gottschalk S, Ng CY, Perez M, et al : An Epstein-Barr virus deletion mutant associated with fatal lymphoproliferative disease unresponsive to therapy with virus-specific CTLs. Blood, 2001 ; 97 : 835-843

ミスマッチ修復異常によってEBNA-3B蛋白の発現消失を来したと考えられる膿胸関連リンパ腫の1例

高　桑　徹　也

要　　約

膿胸関連リンパ腫（PAL）はEpstein-Barrウイルス（EBV）関連リンパ腫の一つで，免疫能低下などのみられない慢性膿胸の患者において，20年以上の慢性炎症を経て胸腔に発症する。72歳の男性症例から採取された同リンパ腫においてEBVの潜伏遺伝子の発現はEBNA-3B遺伝子を除いて発現が認められた。EBNA-3B蛋白は宿主のCTL応答の標的として働くので，その発現消失は，免疫監視機構を回避し腫瘍増殖に有利に働いた可能性がある。EBNA-3B遺伝子の塩基配列を検討すると単塩基重複配列部分に塩基の欠失がみられた。このような欠失はミスマッチ修復異常（MMR type）により生じることが知られ，同腫瘍細胞もMMR typeであった。宿主のMMR typeが感染したEBVゲノム変異に影響を及ぼした点は大変興味深い。

1

Introduction – Developmental Overview of the Human Embryo

Shigehito Yamada[1], and Tetsuya Takakuwa[2]
[1]*Congenital Anomaly Research Center, Kyoto University,*
[2]*Human Health Science, Kyoto University,*
Japan

1. Introduction

In this chapter, we provide a historical background on human embryo collections and describe their significant contribution to the understanding of human ontogenesis. More particularly, an overview of human embryonic development is presented using computer-generated images obtained from embryonic specimens housed at the Kyoto Collection in Japan.

1.1 Human embryology and embryo collections

Historically, several human embryo collections have been created. The Carnegie Collection, the Blechschmidt Collection, the Hinrichsen Collection and the Kyoto Collection are reported as the four famous compendiums of human embryos in the world. The Carnegie Collection is the oldest and was established as early as 1887, while the Blechschmidt collection was created in 1948 by the Göttingen anatomist Erich Blechschmidt, well known for its contribution to the development of novel methods of reconstruction. In 1961, the Kyoto Collection of Human Embryos was instigated, followed by the Hinrichsen Collection in 1969. While the Blechschmidt and the Hinrichsen collections are described in Chapter 2, here, we focus on the Carnegie and the Kyoto Collections.

1.2 The carnegie human embryo collection

The basis of the Carnegie Human Embryo Collection was established by Franklin P. Mall. After earning his medical degree at the University of Michigan in 1883, Mall traveled to Germany to receive a clinical training and there he met Wilhelm His and other eminent biologists. Mall then became aware of the importance of studying human embryology, and initiated a collection of human embryos in 1887. When he returned to the United States and took on a position in the Anatomy department of the Johns Hopkins School of Medicine in Baltimore, Maryland, he already had in his possession several hundreds of specimens. In 1913, as a professor of Anatomy at the Johns Hopkins School of Medicine, Mall applied for a Carnegie grant to support his research on human embryos, was successful in his application and thus, in 1914, became the first director of the Department of Embryology at the Carnegie Institution of Washington, in Baltimore, MD. The collection grew up at a rate of about 400

specimens a year, and the number of samples attained over 8,000 by the early 1940s. The most difficult task, however, was to organize and catalogue the collection. Age or size proved to be a poor way to organize embryos, as embryos could shrink a full 50% in the preserving fluids. Mall devised a better way and based his staging scheme on morphological characteristics instead. To that end, Mall and his colleagues not only prepared and preserved serial sections of the embryos; they also made hundreds of three-dimensional models at different stages of growth. Over 700 wax-based reconstructions were created.

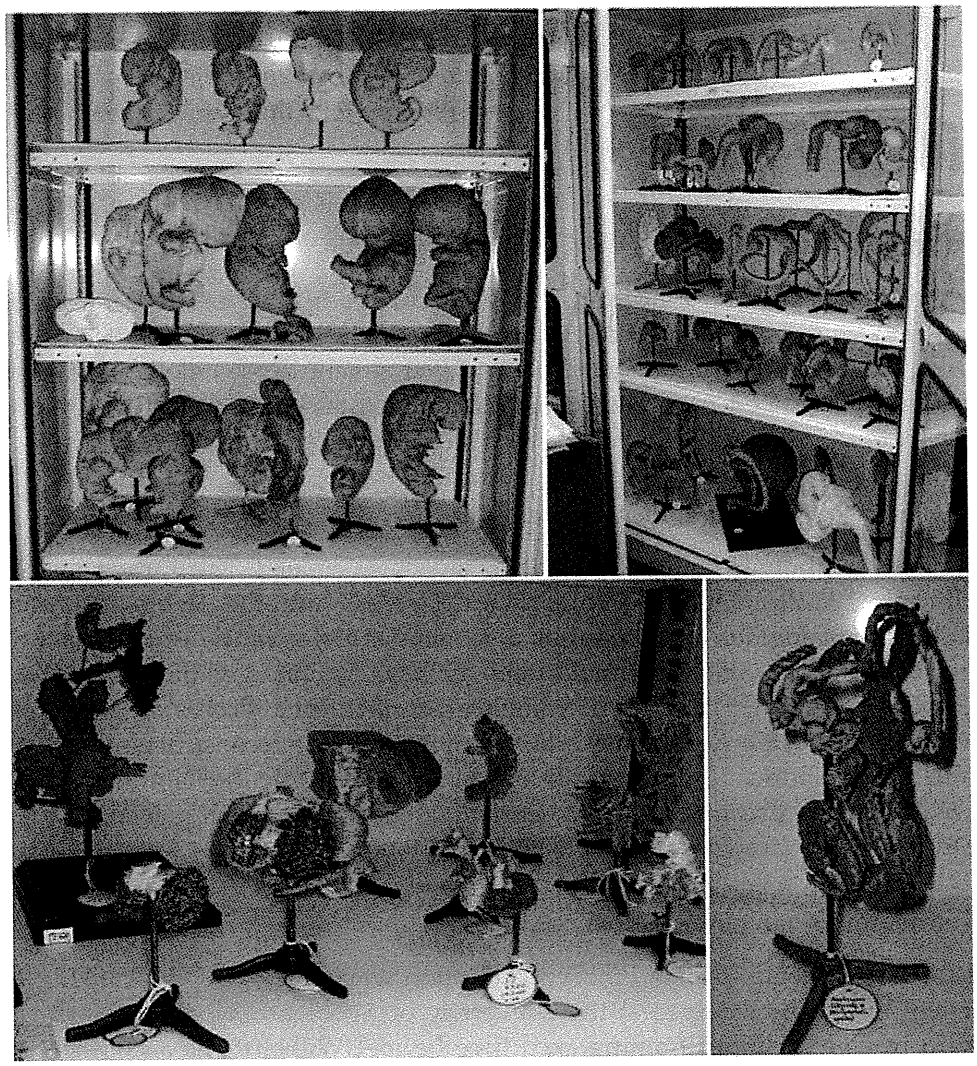

Fig. 1. Wax reconstruction models at the Carnegie Collection, housed at the National Museum of Health and Medicine, Washington, DC. Surface reconstruction of human whole embryos (top left), neural tubes and brains (top right), hearts and great vessels (bottom left), and membranous labyrinth and perilymphatic spaces (bottom right).

Throughout the Mall's era, several members of his department became renowned scientists. George L. Streeter and Franz J. Keibel were both former students of Wilhelm His; Osborne O. Heard worked as an embryo modeler; and James D. Didusch as a scientific

illustrator. Mall documented his research in a series of papers compiled in the *Contributions to Embryology of the Carnegie Institution of Washington*, published from 1915 to 1966. Today, these articles are still regarded as textual and visual standards for human embryologists. In 1917, Mall unexpectedly died, and Streeter became the second director of the Department of Embryology. Under his supervision, hundreds of specimens continued to join the collection every year. Notable were the rare, very young normal specimens. At the time, induced abortions were illegal in the United States and miscarriages usually result in abnormal embryos. Streeter was the first to define the 23 Carnegie Stages currently used to classify the developmental stages of the human embryo.

When Streeter retired in 1940, George W. Corner became the third director of the department. Corner was a former Johns Hopkins researcher who discovered the ovarian hormone progesterone. Under his direction, many advances in human reproductive physiology were made. Research in human embryology continued to be actively pursued, but came to an end in 1956 with the succeeding director. In 1973, the Collection was sent to the University of California at Davis Medical School, where the Carnegie Laboratories of Embryology, under the directorship of Ronan O'Rahilly, officially opened in 1976. In 1991, following O'Rahilly's retirement, the collection was donated to the National Museum of Health and Medicine, located at the Walter Reed Army Medical Center in Washington, D.C. The specimens remain available for use by researchers, and are in high demand. Adrianne Noe and colleagues have generated an online database system for easy information access to some 660 embryos from the collection. These embryos were selected to represent the full range of embryonic growth from single cells through to eight weeks of age. The Carnegie Collection forms the centerpiece of the Human Developmental Anatomy Center, and is used by hundreds of researchers every year. Further details of the embryo collection can be found in earlier publications (Brown, 1987, O'Rahilly, 1988) as well as on the web (http://nmhm.washingtondc.museum/ collections/hdac/carnegie_history.htm).

1.3 The Kyoto collection of human embryos

In 1961, Hideo Nishimura, Professor in the Department of Anatomy at Kyoto University School of Medicine, instigated a collection of human conceptuses. Induced abortions were then legal in Japan under the Maternity Protection Law of Japan, therefore, in a great majority of cases; pregnancies were terminated for social reasons during the first trimester. Fifteen years later, the number of specimens reached over 36,000 and the Congenital Anomaly Research Center was created in 1975. Today, the embryo collection comprises over 45,000 specimens, and represents the largest human embryo collection in the world. The specimens were primarily obtained from pregnancies interrupted by dilatation or curettage. Other specimens resulted from spontaneous or threatened abortions. When the aborted materials were brought to our laboratory, the embryos were measured, staged, and examined for gross external abnormalities and signs of intrauterine death under a dissecting microscope. The developmental stage of the embryos (Carnegie stage: CS) was determined according to the criteria proposed by O'Rahilly and Müller (1987). Since the attending obstetricians were not involved in examining the aborted materials, the collection of embryos was not biased by their outcome (e.g., normal or abnormal, live or dead), thus, the embryo collection is considered representative of the total intrauterine population in Japan (Nishimura, 1974, 1975). Using this representative embryo population, it was reported that

the incidence of malformations in embryos were more frequent than that in infants (Nishimura et al., 1968), and that embryos with severe malformations were prone to spontaneous abortion at high rates (Shiota, 1991). Of these embryonic malformations, holoprosencephaly (HPE) was observed at a high frequency in the Kyoto Collection. HPE is a group of malformation characterized by specific dysmorphia of the brain and the face. They are caused by an impaired or incomplete midline cleavage of the prosencephalon into cerebral hemispheres. Although HPE is a rather rare anomaly in newborns (1/10,000-20,000), it is encountered much more frequently (1/250 or more) in the unselected early human embryonic population (Matsunaga and Shiota, 1977). This estimation may be lower than the actual prevalence as milder forms of HPE also exist but are more difficult to diagnose (Yamada et al., 2004, Yamada, 2006). Well-preserved samples were stored and some of them were selected to be sectioned serially; a total of 500 normal embryos and 500 abnormal embryos were stored as complete serial sections, including HPE embryos.

Fig. 2. The Kyoto Collection of Human Embryos. Stock room (top left, top middle), and individual files containing epidemiological data (top right). Histological specimens (middle left, middle right). Digital slide scanners manufactured by Claro Inc. (http://www.claro-inc.com/); LINCE (bottom left) and TOCO (bottom right).

A unique feature of the Kyoto Collection is that maternal epidemiological data and detailed clinical information on the pregnancies were collected in association with every specimen. Based on these epidemiological data, statistical analyses are currently conducted to determine the existence of potential causative links between maternal factors and congenital anomalies (Kameda et al., 2012).

Recently, owing to advances in imaging technologies, embryos can be scanned and 3D digital models can be generated. Using magnetic resonance (MR) microscopes equipped with superconducting magnets ranging from 1.0T to 7.0T, embryos from the Kyoto Collections were imaged (Haishi et al., 2001, Matsuda et al., 2007, Matsuda et al., 2003, Yamada et al., 2010) and morphologically analyzed using 3D reconstruction (Hirose et al., 2011). Episcopic Fluorescence Image Capture (EFIC) and phase-contrast x-ray computed tomography have also been applied to human embryos of the Kyoto Collection (Yamada et al., 2010, Yoneyama et al., 2011). Further details on imaging techniques and reconstruction can be found in Chapter 7. Additionally, a project aiming at digitizing all histological sections comprised in the library is now ongoing. As mentioned earlier, the Kyoto Collection contains a register of 1,000 embryos sectioned serially; half of them are classified as normal and the other half with anomalies. The project is currently focusing on serial sections of normal embryos. Parts of the digitized serial sections are accessible from our website (http://atlas.cac.med.kyoto-u.ac.jp).

2. Human embryonic development

2.1 Developmental overview (Carnegie stages: CS)

Classification into developmental stages is necessary to accurately describe prenatal growth. Embryonic staging of animals was introduced at the end of the 19th century (Hopwood, 2007), and was first applied to human embryology by Mall (1914), as described earlier. At first, human embryos were classified based on their length on the basis of "3-mm stage", but the approach was quickly abandoned due to high inter-individual variations. Subsequently, Streeter (1942, 1945, 1948, 1951) developed a 23-stage developmental scheme of human embryos, commonly known as the Carnegie stages, a staging scheme which remains widely used today. Here below are illustrated all 23 stages using computer graphics either based on photographs acquired in multiple directions, with precise measurements (CS 1-12), or based on data acquired by magnetic resonance microscopy (Yamada et al., 2006, Matsuda et al., 2003).

Relation between the Carnegie stage and estimated age after fertilization (Table 1)

It is accepted that a wide range of normal variations can occur in actual human embryonic age for any given Carnegie stage. The standard criteria proposed by O'Rahilly and Müller (1987) are close to those suggested by Olivier and Pineau (1962). It is also important to point out that Streeter's human series included pathological specimens obtained from spontaneous abortion or ectopic implantation. In the present chapter, the CG models ranging from CS1 to CS11 were based on Carnegie criteria (O'Rahilly and Müller, 1987), while CS13 to CS23 were based on Kyoto Collection samples (Nishimura et al., 1968, Nishimura et al., 1974).

Carnegie stage (CS)	Ovulation age (days)					
	Streeter (1942, 1945, 1948, 1951)	Nishimura (1968, 1974)	Olivier and Pineau (1962)	Iffy et al. (1967)	Jirásek (1971)	O'Rahilly and Müller (1987)
11	24	27	24	-	23-26	23-25
12	26	30	26	-	26-30	25-27
13	28	32	28	28	28-32	28
14	29	34-35	32	32	31-35	32
15	31.5	36	33	34.5	35-38	33
16	33	38	37	37	37-42	37
17	35	40	41	40	42-44	41
18	37	42	44	43	44-48	44
19	39	44	47.5	45	48-51	47-48
20	41	46	50.5	47	51-53	50-51
21	43	48	52	48.5	53-54	52
22	45	50	54	50	54-56	54
23	47	52	56.5	52	56-60	56-57

Table 1. Estimated ovulation age (days) based on developmental stages (CS) of human embryos, according to various authors. Modified from Nishimura (1983).

Carnegie stage 1: Fertilized ovum
1 day after fertilization, 0.1 mm in diameter

The oocyte is 120-150 μm in diameter and is surrounded by the zona pellucida. The second maturation division of the oocyte completes as the sperm penetrates the egg (fertilization). The sperm head and the nucleus of the oocyte then swell to form the male and female pronuclei, respectively. Once they unite, the resultant diploid cell is called the zygote. The first mitotic division soon begins.

Carnegie stage 2: Cleavage
1.5-3 days after fertilization, 0.1-0.2 mm in diameter

The conceptus is composed of two to 16 cells but has no blastocystic cavity yet and the zona pellucida can still be easily recognized. The size of the embryo is 0.1-0.2 mm in diameter. The cell division at this stage is called cleavage since furrows (clefts) appear as the cytoplasm divides. The daughter cells are called blastomeres. An embryo with 16-32 cells is called a morula.

Carnegie stage 3: Free blastocyst
4 days after fertilization, 0.1-0.2 mm in diameter

The conceptus is a free (unattached) blastocyst. The blastocyst is a hollow mass of cells characterized by the blastocystic cavity. The blastocystic cavity begins by the coalescence of intercellular spaces when the embryo has acquired about 32 cells. The blastomeres segregate into an internally situated inner cell mass and an outer trophoblast. The trophoblast cells form an epithelial arrangement with tight junctions.

Carnegie stage 4: Attaching blastocyst
5-6 days after fertilization, 0.1-0.2 mm in diameter

This stage is characterized by the attached blastocyst, which corresponds to the onset of implantation. Attachment of the embryo occurs only once the endometrium has entered the secretory phase. At the site of attachment, the trophoblast cells are transformed into a

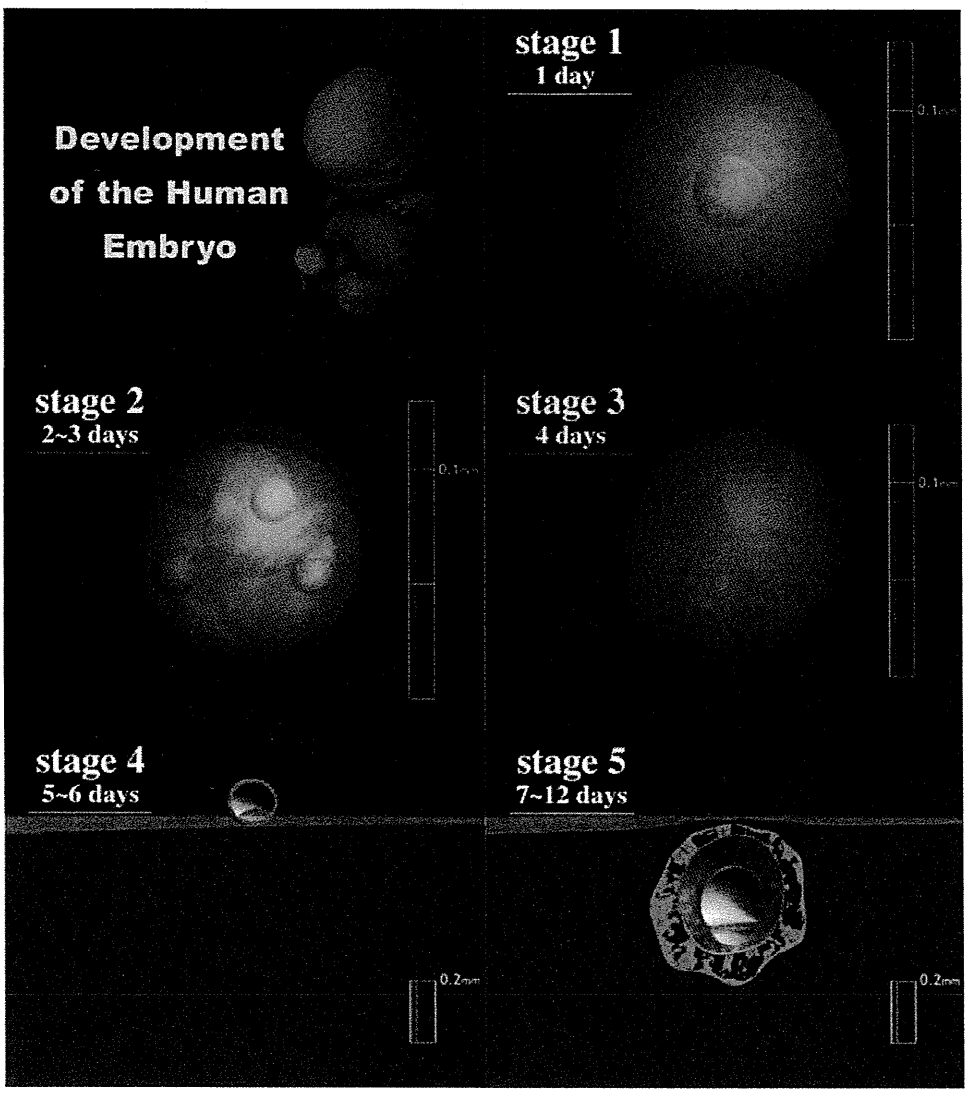

Fig. 3. Computer graphics illustrating embryonic human development: Carnegie stage 1-5.
syncytium and penetrate into the endometrial epithelium.

Carnegie stage 4: Attaching blastocyst
5-6 days after fertilization, 0.1-0.2 mm in diameter

This stage is characterized by the attached blastocyst, which corresponds to the onset of implantation. Attachment of the embryo occurs only once the endometrium has entered the secretory phase. At the site of attachment, the trophoblast cells are transformed into a syncytium and penetrate into the endometrial epithelium.

Carnegie stage 5: Implanted but previllous
7-12 days after fertilization, 0.1-0.2 mm in diameter

The blastocyst penetrates into the endometrium. The trophoblast grows rapidly but is previllous, i.e., it does not yet show definite chorionic villi. This stage is sub-divided into 3 stages according to the differentiation status of the trophoblast: solid trophoblast (stage 5a), lacunar trophoblast (5b), and perfusion of lacunae with maternal blood (5c).

Carnegie stage 6: Chorionic villi and primitive streak
13 days after fertilization, 0.2 mm in size

Chorionic villi appear and begin to branch. Trophoblastic lacunae coalesce to form the intervillous space (6a). The extra-embryonic mesoderm arises and the chorionic cavity is formed. The yolk sac is now called the secondary (definitive) yolk sac. The primitive streak appears later during this stage (6b, "stage 6" in Fig. 2).

Carnegie stage 7: Notochordal process
16 days after fertilization, 0.4 mm in length (embryonic disc)

The notochordal process develops in the mesodermal layer rostral to the primitive node. The length of the notochordal process varies from 0.03 to about 0.3 mm. The embryonic mesoderm spreads laterally and rostrally from the primitive streak. The embryonic disc grows cranially and the amniotic cavity expands over the yolk sac.

Carnegie stage 8 : Primitive pit, neuenteric canal
18 days after fertilization, 1.0 mm in CRL (crown-rump length)

This stage is characterized by the formation of the primitive pit, the notochordal canal and the neurenteric canal. Somites are not yet visible (presomitic stage). The embryonic disc is pyriform, tapering caudally. The notochordal canal is marked by the cavity extending from the primitive pit into the notochordal process. The floor of the canal soon disappears to form a passage between the amniotic cavity and the yolk sac (neurenteric canal).

Carnegie stage 9: 1-3 pairs of somites
20 days after fertilization, 1.5 mm in CRL

The neural groove and the first somites appear, and one to three pairs of somites can be observed. The embryonic disc resembles a shoe-sole, with the broad neural plate positioned into the cranial region. The neural groove appears during this stage and subsequently deepens. The paraxial mesoderm becomes segmented to form somites.

Carnegie stage 10: Neural folds begin to fuse, 4-12 pairs of somites
22 days after fertilization, 1.8 mm in CRL

The neural groove deepens and the neural folds begin to fuse to form the neural tube. The fusion of neural folds extends bidirectionally. The optic sulcus and branchial arch 1 (i.e., pharyngeal arch) begin to be visible. The cardiac loop starts to appear.

Carnegie stage 11: Anterior neuropore closes
24 days after fertilization, 2.5-3 mm in CRL

The human embryo now has 13-20 pairs of somites. The anterior neuropore is now closing up. Optic evagination is produced at the optic sulcus and the optic ventricle is continuous with that of the forebrain. The sinus venosus develops in the cardiac loop. The